Morphological and Rheological Responses to Shear Start-up and Flow Reversal of Thermotropic Liquid-Crystalline Polymers

Patrick T. Mather,*,†,‖ Hong G. Jeon,‡ Chang Dae Han,*,§ and Sukky Chang§

Air Force Research Laboratory and Systran Corporation, Materials and Manufacturing Directorate, AFRL/MLBP, 2941 P Street, Wright Patterson AFB, Ohio 45433-7750, and Department of Polymer Engineering, The University of Akron, Akron, Ohio 44325-0301

Received May 3, 2000; Revised Manuscript Received July 27, 2000

ABSTRACT: Novel rheo-optical methods have been used to directly observe morphology evolution, during shear start-up and reversal flow, in semiflexible main-chain thermotropic liquid-crystalline polymers (TLCPs). Using a specially designed microrheometer allowing for simultaneous transient optical and mechanical observations, we observed band formation upon reversal of flow direction. It was seen that this band formation causes asymmetric light diffraction in H_V small-angle light scattering mode, indicating a tilted arrangement of the regularly spaced bands. Also conducted were shear start-up and flow reversal experiments using a cone-and-plate rheometer under the same thermal and deformation histories as those in rheo-optical experiments for polymers of differing spacer lengths at equal temperature difference below the nematic-to-isotropic transition temperature (T_{NI}). It was observed that, during both shear start-up and flow reversal, the first normal stress difference $N_1^+(\dot\gamma, t)$ exhibits a large overshoot followed by an oscillatory decay, while shear stress $\sigma^+(\dot\gamma, t)$ exhibits a large overshoot followed by a monotonic decay. It was found that the higher the applied shear rate, the larger the overshoot of $N_1^+(\dot\gamma, t)$ and $\sigma^+(\dot\gamma, t)$, and the longer the persistence of oscillations in $N_1^+(\dot\gamma, t)$. Similarity was found between the ratio $N_1^+(\dot\gamma, t)/\sigma^+(\dot\gamma, t)$ and flow birefringence $\Delta n^+(\dot\gamma, t)$ during shear start-up and flow reversal of the TLCPs investigated in this study. Further, we found that the ratio $\sigma^+(t,\dot\gamma)/\sigma$ scales with $\dot\gamma t$ but the ratio $N_1^+(\dot\gamma, t)/N_1$ does not, where σ denotes shear stress at steady state and N_1 denotes first normal stress difference at steady state.

1. Introduction

Orientational banding in liquid-crystalline polymers (LCPs) is a ubiquitous phenomenon[1−8] that, while scientifically intriguing, is detrimental to the mechanical properties.[1] Banding phenomena in LCPs generally result from reorientation of the average molecular orientation (director) driven either by a prescribed mechanical deformation, magnetic or electric field, or by relaxation of elastic energy stored in the material during flow or deformation. The bands are always found to be perpendicular to the average orientation direction (prior to band formation) and are easily visualized with polarizing optical microscopy (POM), due to the large birefringence of LCPs, as well as with transmission electron microscopy.

While relaxation following shear cessation leads to band formation perpendicular to the flow direction, flow or deformation orthogonal to the bulk orientation (or previous deformation direction) leads to bands *parallel* to the second deformation direction. Maffettone et al.[5] found that, for a lyotropic LCP, application of a second shear in the orthogonal direction resulted in the formation of bands oriented perpendicular to the original shear direction, but parallel to the second shear direction. The origin of this pattern formation is distinct from that of the more commonly seen bands and is likely an optical manifestation of a "roll-cell" structure predicted by Pieranski and Guyon,[9] Manneville and Dubois-Violette,[10] and later studied by Larson.[11] In a similar fashion, when monodomain liquid-crystalline elastomers are drawn in a direction orthogonal to the monodomain director, the same type of bands forms parallel to the drawing direction.[8] In this case, however, the mechanism of band formation appears to be distinct from roll-cell formation intrinsic to "tumbling" nematics and has been described[12] as an energy balance between the director inversion wall creation and the imposed mechanical constraint of the drawing process.

Almost all research on band formation in LCPs has focused on experimental observations while little theoretical work has been pursued. Some important work by Han and Rey,[13] however, has focused on the mechanism of band formation in simple shear flow. In particular, Han and Rey have found from simulations of the Leslie−Ericksen theory that shear start-up of a "tumbling" nematic initially oriented homeotropically leads to the nucleation of *tilted tubular inversion walls*, which are oriented orthogonal to the velocity and velocity gradient directions. In these predicted structures, the bulk orientation (in a snapshot of time) is in the flow direction, as is the material within the tubes. However, the tubes are defined by inversion walls where dramatic reorientation of the director from the bulk region to the tube interior occurs by an angle of π. Importantly, Han and Rey found that the tubular inversion walls are compliant and susceptible to tilting toward the flow direction; i.e., the tube cross section becomes ellipsoidal and oriented in the flow direction.

The response of LCPs to a reversal in shearing flow direction has been studied experimentally[14−17] and theoretically[18] to reveal significant and long-lived orientational disruptions. Experiments have shown a strong oscillatory response of optical birefringence[15] and

* To whom correspondence should be addressed.
† Air Force Research Laboratory, AFRL/MLBP.
‡ Systran Corporation, AFRL/MLBP.
§ The University of Akron.
‖ Present address: Institute of Materials Science and Chemical Engineering Dept., University of Connecticut, Storrs, CT 06269.

10.1021/ma000765r CCC: $19.00
Published on Web 10/03/2000

dichroism[14] to flow reversal for lyotropic solutions. To the best of our knowledge, however, no rheo-optical investigation of thermotropic liquid-crystalline polymers (TLCPs) in reversal flow has been reported. In Semenov's theoretical study[18] on oscillatory shear flow, it was reported that "texture formation" is expected when the nematic is flow-aligning and the shear strain amplitude is sufficiently large, for a two-dimensional calculation with the Leslie−Ericksen theory. More specifically, Semenov[18] proposed that thermal fluctuations may lead to a splitting of director rotation into domains with the director of some domains rotating in the shearing plane, against vorticity, through a small angle ($2\theta_L$) while the directors in other domains rotate with vorticity through a larger angle, $\pi - 2\theta_L$. Here, θ_L is the Leslie angle corresponding to the steady-state angle achieved between the director and the flow axis for flow-aligning nematics.

Using flow birefringence, Hongladarom et al.[15] investigated the degree of molecular orientation in transient shear flow of a lyotropic solution of poly(benzyl glutamate) (PBG) at low shear rates. They observed that damped oscillations in birefringence, scaling with strain, resulted from a reversal in shear flow direction as predicted by the Larson−Doi polydomain model.[19] They observed even stronger oscillations in flow reversal, which is in agreement with the model prediction. However, they noted an initial increase in oscillation amplitude along the flow direction following flow reversal, in contrast to the model prediction. It was speculated that the observed discrepancy between experiment and model prediction might be an indication that the steady-state domain orientation distribution predicted by the model does not capture the detailed structure of PBG solutions sheared at low shear rates.

Earlier, Han and co-workers investigated shear start-up,[20−22] intermittent shear flow,[23] and stress relaxation upon cessation of shear flow[24] of a semiflexible main-chain TLCP, poly[(phenylsulfonyl)-*p*-phenylene decamethylene bis(4-oxybenzoate)]s (PSHQ10) having the

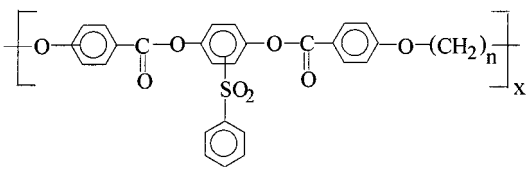

chemical structure shown here, with $n = 10$. More recently, Chang and Han[25] investigated the influence of the spacer length on shear start-up (shear stress and first normal stress difference) as well as the effect of temperature for a homologous series of PSHQ*n* with *n* varying from 3 to 12. Broadly speaking, these model TLCPs show a rich range of reproducible rheological responses generally suggesting flow-aligning behavior.

In the present study, we observed, via in-situ polarizing optical microscopy and conoscopic small-angle light scattering, band formation in the PSHQ*n* following a reversal in the shearing flow direction. For the investigation we have used our unique optical microrheometer to examine *simultaneously* the macroscopic shear stress and optical response (birefringence, microscopy, light scattering) during shear start-up and flow reversal. Also, we used a cone-and-plate rheometer to investigate shear start-up and flow reversal of PSHQ*n*. Upon flow reversal of PSHQ*n*, we observed oscillatory behavior in the first normal stress difference, very similar to that observed in flow birefringence using the optical microrheometer. The paper is organized as follows. We first present our experimental results of the morphology evolution in PSHQ*n* during shear start-up and flow reversal and then offer, with the aid of independent measurements of shear stress and first normal stress difference from a cone-and-plate rheometer, an explanation for the origin of the band formation during flow reversal. Finally, we summarize the rich morphological and rheological behavior that should be captured in the future by a successful theory of thermotropic polymer rheology.

Table 1. Summary of the Intrinsic Viscosities and Transition Temperatures of PSHQ*n* Investigated in This Study

polymer	$[\eta]$ (dL/g)[a]	T_g (°C)	T_{NI} (°C)	mesophase
PSHQ6	0.877	110	228	nematic
PSHQ10	0.667	92	181	nematic
PSHQ11	0.485	77	147	nematic

[a] $[\eta]$ was measured on 1,1,2,2-tetrachloroethane at 23 °C using an Ubbelohde viscometer.

2. Experimental Section

2.1. Materials. In this study we used PSHQ6, PSHQ10, and PSHQ11, the chemical structures of which are given above. Note that the number at the end of PSHQ refers to the number of methylene groups present in PSHQ*n*. The details of synthesis procedures for PSHQ*n* are given elsewhere.[26,27]

The intrinsic viscosity ($[\eta]$), glass transition temperature (T_g), and nematic-to-isotropic transition temperature (T_{NI}) of the PSHQ*n* employed in this study are summarized in Table 1.[28]

We emphasize at this juncture that the rheological behavior of TLCPs, existing in an orientationally anisotropic state, depends very much on previous thermal and deformation histories.[29,30] Thus, control over the initial conditions of TLCP specimens is critical for obtaining *reproducible* rheological responses.[20−22,31] Our approach toward controlling initial conditions is to first heat samples above an isotropization temperature without thermal degradation, implying the need for specimens having isotropization temperatures sufficiently below the thermal degradation temperatures. It was reported[28] that PSHQ*n*'s undergo thermal degradation at approximately 350 °C, well above T_{NI}. Therefore, each of the PSHQ*n*'s employed in this study enabled us to first erase previous thermal and morphological history by heating above T_{NI} (without thermal degradation) and then cool to a predetermined temperature in the nematic region. Specifically, each specimen was first cleared upon loading by heating to T_{NI} + 20 °C, followed by cooling to either T_{NI} − 20 °C or T_{NI} − 40 °C before conducting shear start-up and flow reversal experiments.

2.2. Sample Preparation. Specimens for rheo-optical and shear rheometric experiments were prepared by first dissolving each polymer in dichloromethane (for PSHQ10 and PSHQ11) or tetrachloroethane (for PSHQ6) in the presence of 0.1 wt % antioxidant (Irganox 1010, Ciba-Geigy Group) and then slowly evaporating the solvent at room temperature for 1 week. The cast films (1-mm thick) were further dried in a vacuum oven at room temperature for at least 3 weeks and, prior to measurements, at 90 °C for 48 h to remove any residual solvent and moisture. For rheo-optical experiments, small portions (25−100 mg) of the cast films thus prepared were melted onto one glass plate of the rheometer and carefully consolidated to a thin strand, approximately 1 mm in width, along the optical access slit and subsequently cycled several times through a spatula compression/annealing process to aid in void elimination. Finally, the polymer strands were vacuum-treated at T_{NI} − 20 °C for a period of 60 min to remove any remaining voids introduced during sample preparation.

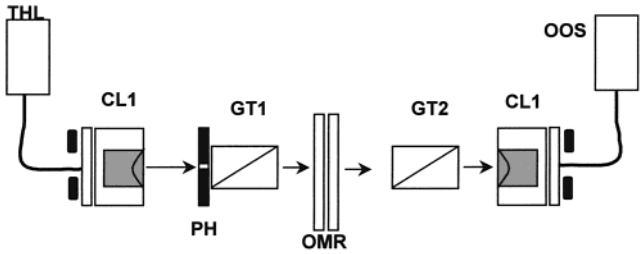

Figure 1. Schematic describing the optical microrheometer apparatus combined with spectrographic birefringence optics. Light from a tungsten−halogen fiber-optic source (THL) is focused on the sample (OMR), using a 10-cm focal-length lens (CL1), transmitted through a pinhole (PH), and polarized using a Glan-Thompson polarizer oriented 45° from the flow axis (GT1). Transmitted light passes through an analyzer oriented parallel to the polarizer (GT2) and is collected by a second lens (CL2) and fiber-optic assembly where it is connected to the Ocean Optics spectrometer (OOS) for analysis.

2.3. Optical Microrheometry (OMR). The optical microrheometer employed for this study has been previously described in some detail.[32,33] The rheometer features computer-controlled shearing flow between parallel quartz plates at elevated temperature with provision for shear stress measurement. For future reference, the flow direction is **1**, the velocity gradient direction is **2**, and the vorticity direction is **3**. The shear stress measurement is made on the basis of the total lateral force on the stationary plate divided by the sample area, which is determined, in all cases, using calibrated image processing[34] after the experiments are completed and the shear cell is opened. Unless otherwise noted, the sample thickness is 50.8 μm.

We expected that the birefringence of our thermotropic polymers should be large and comparable to values for small molecule nematics ($\Delta n \sim 0.1$) so that, for the sample thicknesses used in the experiments, retardances in the range of 5000 nm would result. These retardance values are far in excess of the values accessible using standard polarimetry methods; therefore, we have adopted the method of spectrographic birefringence first introduced for analysis of lyotropic LCPs by Hongladarom et al.[35] and later employed Beekmans and Posthuma de Boer[36] for ex-situ analysis of solid thermotropic LCP films. To the best of our knowledge, however, spectrographic birefringence has not been previously applied to in-situ measurements on flowing TLCPs, presumably due to difficulties in providing controlled shearing of samples with sufficiently small thicknesses (<100 μm) to overcome the effects of sample turbidity. The optical train for our spectrographic birefringence setup is shown in Figure 1. White light from a tungsten lamp (THL; LS-1, Ocean Optics) is coupled to a fiber optic cable, the emerging light beam collimated using an objective lens (CL1), and the light transmitted through the sample shearing plane (OMR). Between the incident collimating lens and the optical microrheometer is a Glan-Thompson polarizer (GT1) to achieve linear polarization (>7000:1) oriented 45° away from the flow axis. The polarized and collimated light that passes through the shearing cell and sample then passes through a second Glan-Thompson polarizer (analyzer, GT2) oriented parallel to the incident polarizer. Finally, the analyzed light is collected with a receiving objective lens (CL2) mated with a fiber optic cable, terminating at a visible spectrometer (OOS).

Specifically, the received light is then analyzed for its spectral content using an Ocean Optics spectrometer (S2000) and OOIBase software. The raw intensity spectra were normalized using the following formula,

$$T_{\parallel}(\lambda) = (I(\lambda) - I_d(\lambda))/(I_o(\lambda) - I_d(\lambda)) \quad (1)$$

where $I_o(\lambda)$ is the spectrum of the unoriented polymers in the isotropic phase and $I_d(\lambda)$ is the dark spectrum obtained when the light source is blocked. By making use of the bright transmission spectrum of the isotropic polymer, we are able to factor out the lightly wavelength-dependent absorption of the polymer, which is largely independent of orientation, thus avoiding the need for two observations (parallel and crossed polarizers), previously adopted,[15,36] for each birefringence measurement.

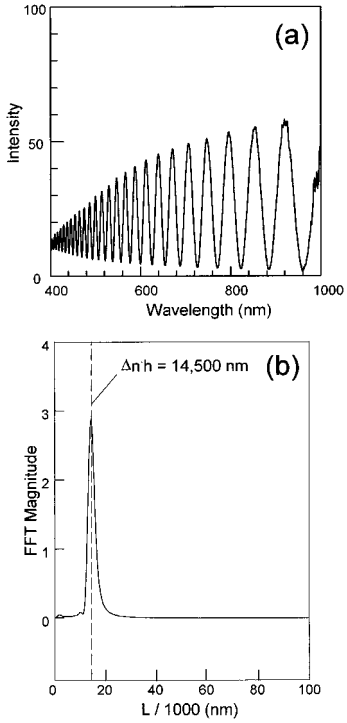

Figure 2. (a) Example of raw visible spectrum, $T_{\parallel}(\lambda)$, from a shear-aligned sample of PSHQ11. (b) Results of the fast Fourier transform of $T_{\parallel}(L)$ used to extract the sample birefringence.

For parallel polarizers, the measured transmission spectra are given as[37]

$$T_{\parallel}(\lambda) = A \cos^2\left(\frac{\pi \Delta n h}{\lambda}\right) \quad (2)$$

where Δn is the birefringence projected on the velocity−vorticity plane, or Δn_{13}. Hongladarom et al.[15] analyzed data following a similar expression by nonlinear regression of the spectral data with a high-order polynomial description of the apparent dispersion in birefringence. Following an alternative method, Beekmans et al.[36] employed the large number of oscillations in their measured spectra and extracted birefringence from the fringe spacing. Both methods have respective advantages, but require significant user intervention during data analysis. We have adopted a new approach to the analysis of data using eq 2, in which a selected spectral window of data, namely, $575 < \lambda < 775$ nm, is analyzed using a fast Fourier transform (FFT). For this purpose, the transmission spectra data sets are interpolated to yield even spacing on the ordinate ($L = 1/\lambda$), convoluted with a Hanning window, and padded with zeroes to 4096 data points. The FFT of data sets prepared in this way leads to a narrow peak in the power spectrum at $L = \Delta n h$, the retardance of the sample. Calibration of the spectrometer, including the numerical processing, was confirmed using multiorder retarders with known retardance (Melles Griot, Newport Corp.).

Figure 2 gives an example analysis of spectrographic data for an oriented sample of PSHQ11. Figure 2a shows the strong oscillations in transmission spectrum, $T_{\parallel}(\lambda)$ (corresponding to the function in eq 2), convoluted with an amplitude envelope. This envelope has a magnitude <1 and shows a significant decrease in transmission as shorter wavelengths are approached. The former effect (magnitude) is strongly connected to the defect texture of the material through scattering-based turbidity, but also through polarization state mixing.[15] We

attribute the decreasing transmission at short wavelengths to significant polarized absorption in the ordered, nematic phase. The power spectrum of the data shown in Figure 2a, computed using a FFT, is given in Figure 2b where a narrow peak centered at $L = 14\,500$ nm is found. The square root of the peak magnitude is equivalent to the amplitude of the spectral oscillations and is referred to as A_S below. Thus, the measurement of birefringence reduces to simple peak searching of rapidly computed FFT power spectra.

2.4. Polarizing Optical Microscopy (POM). POM images were collected using an Aus Jena polarizing microscope with a long working distance objective lens (25×) in which the crossed polarizers were arranged with the polarizer either parallel to the flow direction (H_V POM) or at an angle 45° to the flow direction. POM images were recorded using a Panasonic KR222 CCD camera (768 × 493 pixel resolution) in conjunction with a JVC HR-S53OOU SVHS video recorder for subsequent digitization using a Data Translation DT3152 frame grabber and *ImageTool* the software.[34] Color photomicrographs were obtained using 800-speed photographic film along with an autoexposure system of the Aus Jena microscope.

2.5. Conoscopic Small-Angle Light Scattering (CSALS). CSALS was performed by passing a narrow beam of green ($\lambda = 530$ nm) or blue ($\lambda = 480$ nm) filtered light through the sample. The light is polarized along the flow direction and the pattern of scattered light imaged using a Bertrand lens with an analyzer crossed with the polarizer (H_V arrangement). The scattering angles for CSALS were calibrated using a Ronchi ruling with 300 lines/mm (American Optical Co., Buffalo, NY). The light scattered by a modulation in refractive index, such as that seen in textured liquid-crystalline materials, is given as[38]

$$I(\mathbf{q}) = KV\langle n^2\rangle \int \gamma(\mathbf{r}) e^{i\mathbf{q}\mathbf{r}}\, d\mathbf{r} \tag{2}$$

where **q** is the scattering vector whose magnitude is defined as

$$\|\mathbf{q}\| = \frac{4\pi}{\lambda}\sin(\theta/2) \tag{3}$$

and

$$\gamma(\mathbf{r}) = \frac{\langle n_i n_j\rangle}{\langle n^2\rangle_{avg}} \tag{4}$$

is the spatial correlation of the refractive index in the medium normalized by the mean square variation in the refractive index, $\langle n^2\rangle$. In eq 2, K is a constant, V is the scattering volume, and **r** is the spatial coordinate. Therefore, it is anticipated that by inspecting the CSALS pattern, we gain insight regarding the domain texture of the samples.

In the simple case of periodic, one-dimensional variation in a refractive index of sufficient magnitude, diffraction according to eq 5 (Bragg's Law in transmission) is expected. Here, d

$$d \sin\theta = m\lambda \tag{5}$$

refers to the period of the refractive index, θ is the diffraction angle, m is the diffraction order, and λ is the wavelength of light being diffracted.

2.6. Cone-and-Plate Shear Rheometry. A Rheometrics mechanical spectrometer (RMS Model 800) with a cone-and-plate (8-mm-diameter plate, 0.1-rad cone angle) fixture was used to measure, during shear start-up, the shear stress growth $\sigma^+(t, \dot\gamma)$ and first normal stress difference growth $N_1^+(t, \dot\gamma)$ as functions of time (t) for various shear rates ($\dot\gamma$) and temperatures. Because the RMS 800 did not allow us to conduct reversal flow experiments without a finite delay time between flow directions, an ARES model rheometer with a cone-and-plate (8-mm-diameter plate, 0.1-rad cone angle) fixture (Rheometric Scientific Inc.) was used to conduct continuously both shear start-up and flow reversal experiments without stopping flow. For the rheological measurements, specimens were first heated to the isotropic state (T_{NI} + 20 °C), kept there for about 10 min under shearing at $\dot\gamma = 0.1\ s^{-1}$, and then cooled to a predetermined temperature (T_{NI} − 20 °C or T_{NI} − 40 °C) in the nematic region. Shear start-up experiments began after temperature equilibration in the nematic region. In conducting the flow reversal experiment using ARES, the shear direction was reversed suddenly, without stopping flow, after 200 strain units during forward shear flow. All experiments were conducted under a nitrogen atmosphere to minimize oxidative degradation of the specimens. Temperature control was satisfactory to within ±1 °C.

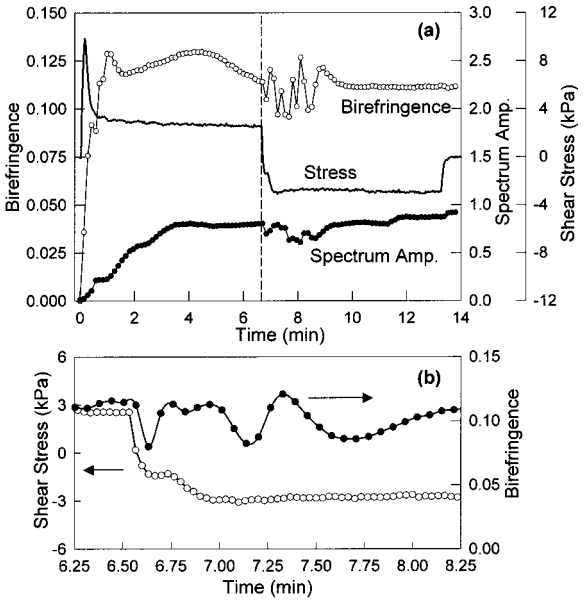

Figure 3. (a) Time evolution of birefringence (○), spectrum amplitude (●), and shear stress (solid line) during shear start-up and flow reversal of PSHQ10 at 160 °C and at $\dot\gamma = 0.5\ s^{-1}$. Sample thickness is 50.8 μm. (b) Expanded time scale of flow reversal of PSHQ10 under the same conditions.

3. Results and Discussion

The shearing temperatures employed for PSHQ10, PSHQ11, and PSHQ6 were T_{NI} − 20 °C and/or T_{NI} − 40 °C for each polymer. The choice of shearing temperature at T_{NI} − 20 °C results in variation in another temperature parameter, namely, $T - T_g$, which is ≈68, 50, and 100 °C for PSHQ10, PSHQ11, and PSHQ6, respectively (see Table 1). We will show below that this variation leads to strongly varying shear stress levels between samples at the same shear rates, which will be taken into consideration in describing the orientation development during shear start-up. It should be noted, however, that a previous study[25] has shown a specific odd−even influence on the nematic viscosity in which odd-numbered PSHQ*n*'s have generally higher steady-state shear viscosities than their even-numbered counterparts of comparable molecular weight. This effect makes it impossible to choose a temperature above T_g in the nematic phase, providing equivalent steady-state shear viscosities.

3.1. Microstructural Evolution during Shear Start-up. Figure 3 gives plots of birefringence ($\Delta n^+(\dot\gamma, t)$), transmission spectrum amplitude ($A_S^+(\dot\gamma, t)$), and shear stress ($\sigma^+(\dot\gamma, t)$) versus time for PSHQ10 during start-up of shear flow and subsequent flow reversal at 160 °C and at $\dot\gamma = 0.5\ s^{-1}$. Notice in Figure 3 that the peak value of $\sigma^+(\dot\gamma, t)$ is about 4 times the steady-state value, σ, prior to flow reversal. The large overshoot in

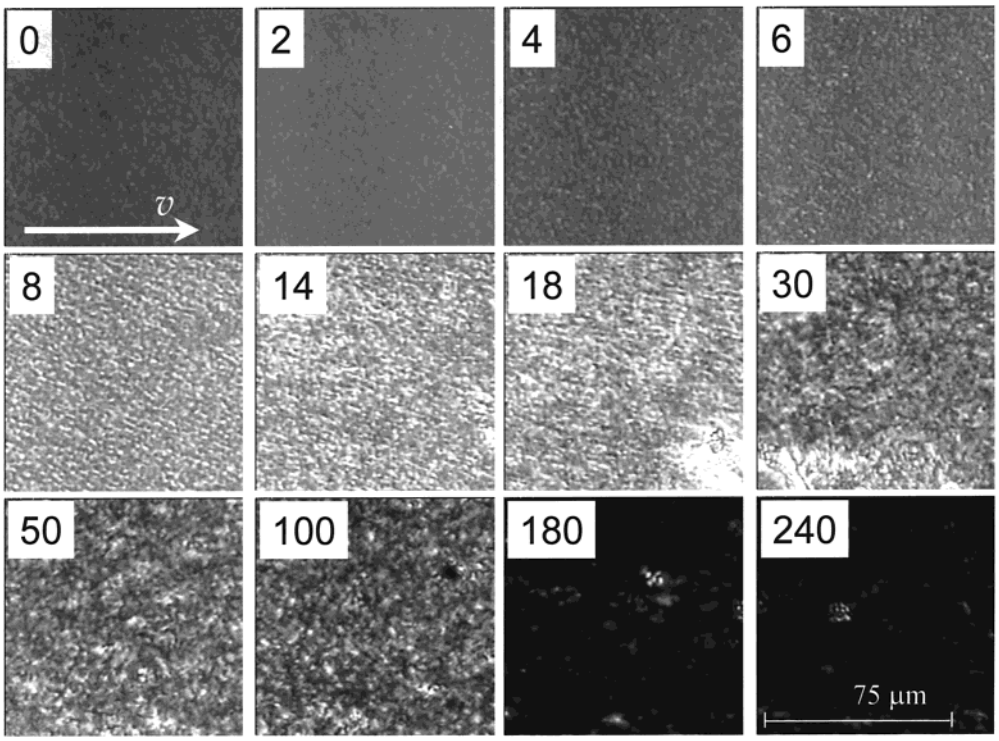

Figure 4. Time evolution of the POM image during start-up shear flow of PSHQ10 at 160 °C and $\dot{\gamma} = 0.5\ s^{-1}$. The optics are arranged with the flow direction from left to right, white light polarized parallel to the flow direction, and the analyzer crossed with the polarizer. The observation times in seconds are shown in the upper left of each POM image. Sample thickness is 50.8 μm.

$\sigma^+(\dot{\gamma}, t)$ has been observed previously[20−22,25] for PSHQ10 and is attributed to the tight defect texture resulting from nematic nucleation from the isotropic phase.[39] In contrast to $\sigma^+(\dot{\gamma}, t)$, the birefringence evolution during start-up shear flow, $\Delta n^+(\dot{\gamma}, t)$, shows a growth from near zero to a relatively delayed maximum occurring at $\dot{\gamma}t \sim$ 30−40 strain units, followed by a long period of oscillation spanning several minutes up to the point of flow reversal. The spectrum amplitude, $A_S{}^+(\dot{\gamma}, t)$, on the other hand, develops in a manner that is ostensibly independent of the birefringence, featuring a period of roughly linear growth during the first 60 strain units, after which an asymptote of $A_S = 0.9$ is reached.

To supplement the macroscopic $\Delta n^+(\dot{\gamma}, t)$ and $\sigma^+(\dot{\gamma}, t)$ data of Figure 3, which reflect both molecular and textural order, with morphological observations, we present in Figure 4 *direct* POM images with reference to $\sigma^+(\dot{\gamma}, t)$. Here, the incident polarization is oriented along the flow axis and the microscope analyzer is oriented perpendicular to this polarization direction (H_V configuration). The plane imaged is the velocity−vorticity plane and the depth-of-focus is ≈5 μm (∼10% sample thickness). Following the time evolution of the birefringent, defect-ridden, texture indicated by the time captions in each frame, we observe a rich progression of micrometer-scale textures. As was the case for the birefringence and stress measurements (Figure 3), the PSHQ10 specimen was first heated to 200 °C in the isotropic phase where it was annealed for 5 min and subsequently cooled to the test temperature of 160 °C. The specimens were then annealed an additional 5 min to ensure thermal equilibration. This thermal history results in the quite turbid texture shown for $t = 0$ min in Figure 4. In this case, little light is transmitted and the relatively featureless POM image indicates a characteristic texture scale smaller than 2 μm.

Following shear start-up at $\dot{\gamma} = 0.5\ s^{-1}$, the fine texture coarsens gradually during the first 10 s (5 strain units) to yield a more transparent film, indicating less scattering and significant director orientation away from the flow axis (incident polarization direction). The texture contains stretched birefringence domains in an otherwise featureless, still defect-ridden, matrix. For the period from 14 to 30 s following shear commencement, the domains stretch further and appear to break up in a manner akin to droplets in an immiscible blend and coalesce to a much coarser morphology (12−15 μm) with less orientation of the domains themselves. At this stage, the overall level of transmitted intensity is substantial. Gradually, over the next 2−3 min (100 strain units) the overall brightness decreases, indicating continued enhancement of alignment along the flow axis, while the textural length scale remains fairly steady.

The early stages of shear start-up shown in Figures 3 and 4 indicate a strong correlation between the changing nematic microstructure and the large overshoot in $\sigma^+(\dot{\gamma}, t)$, as highlighted in Figure 5. Here, we plot both $\sigma^+(\dot{\gamma}, t)$ and the synchronous H_V POM images following start-up shear flow of PSHQ10 at 160 °C and $\dot{\gamma} = 0.5\ s^{-1}$. During the initial rise of $\sigma^+(\dot{\gamma}, t)$, only moderate disruption to the original texture is observed; however, at the peak value of $\sigma^+(\dot{\gamma}, t)$, there begins a "yielding" of the tight unoriented texture to bright, stretched domains whose orientation and elongation appear to follow the decrease in $\sigma^+(\dot{\gamma}, t)$ toward a steady state with time. This steady state occurs after a strain of ≈50 units.

With the desire to further understand the development of orientation during start-up shear flow of PSHQ10, we have also examined the in-situ CSALS patterns. It should be mentioned that SALS of LCPs

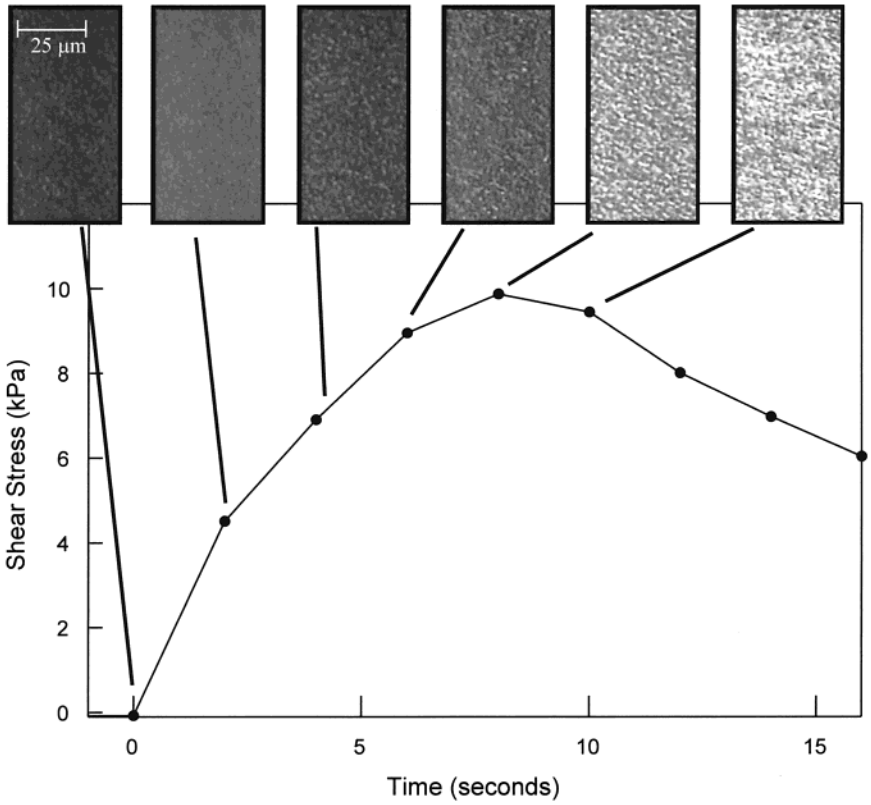

Figure 5. Time evolution of shear stress and POM image of PSHQ10 during the first 15 s following shear start-up at $T = 160$ °C and $\dot{\gamma} = 0.5$ s^{-1}, showing correlation of textural yielding with shear stress maximum.

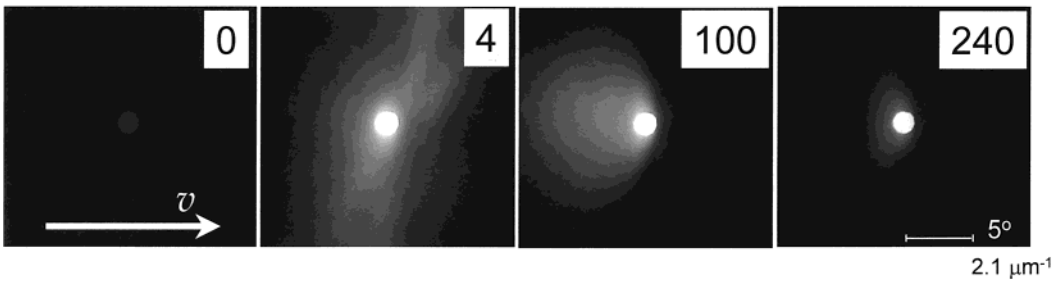

Figure 6. Time evolution of CSALS patterns of PSHQ10 prior to flow reversal. The observation times in seconds are shown in the upper right of each POM image. Sample thickness is 50.8 μm.

has been previously studied by Hsiao et al.,[38] Takebe et al.,[40] Picken et al.,[41] and Walker et al.[42] with the goal of elucidating the influence of shear on microstructure. Figure 6 gives digital snapshots of CSALS patterns for $\dot{\gamma} = 0.5$ s^{-1} at times following shear start-up of 0, 4, 100, and 240 s, corresponding to strains of 0, 2, 50, and 120 strain units. Initially (at $t = 0$ s), the pattern of scattered light in Figure 6 is relatively featureless and is consistent with a highly turbid POM image (see Figure 4 at $t = 0$ s) with significant multiple scattering. After 4 s of shearing, the scattering pattern has changed significantly to yield anisotropic scattering—with a streak appearing perpendicular to flow—indicative of some textural alignment along the flow axis, despite the observation of textural isotropy using POM (see Figure 4 at $t = 4$ s). Following continued shearing, the scattering patterns show enhanced anisotropy for the period ranging from 6 to 50 s, after which the patterns transform to an asymmetric pattern as shown for $t = 100$ s in Figure 6. Here, the asymmetry of the scattering pattern is biased toward scattering away from the flow direction, largely in the plane containing the flow and velocity gradient axes. We tentatively attribute this scattering asymmetry to polarization effects of an apparently tilted texture, noting that great care has been given to ensure that the flow axis and optical axis remain perpendicular. Shearing further still leads, ultimately, to a featureless pattern in which the sheared film is no longer scattering light due to the homogeneity of the sample orientation. This lack of scattering is consistent with the highly oriented and coarsened POM image (see Figure 4 at $t = 240$ s).

3.2. Morphology Evolution during Flow Reversal. With reference to Figure 3, after shearing for 200 strain units at $\dot{\gamma} = 0.5$ s^{-1}, a reversal in the shearing direction leads to significant textural dynamics, which should be considered in light of the $\Delta n^+(\dot{\gamma}, t)$ and $\sigma^+(\dot{\gamma}, t)$ obtained during start-up shear flow. Specifically, upon flow reversal, $\sigma^+(\dot{\gamma}, t)$ immediately changes sign, goes through a weak maximum (or hesitation) after 5 strain units, and subsequently experiences a small primary overshoot before reaching a steady-state value of ≈2.4 kPa and an associated viscosity of 4800 Pa s. This feature is shown more clearly in Figure 3b, where the time scale is expanded and the birefringence data were taken more frequently. We note that the existence of a

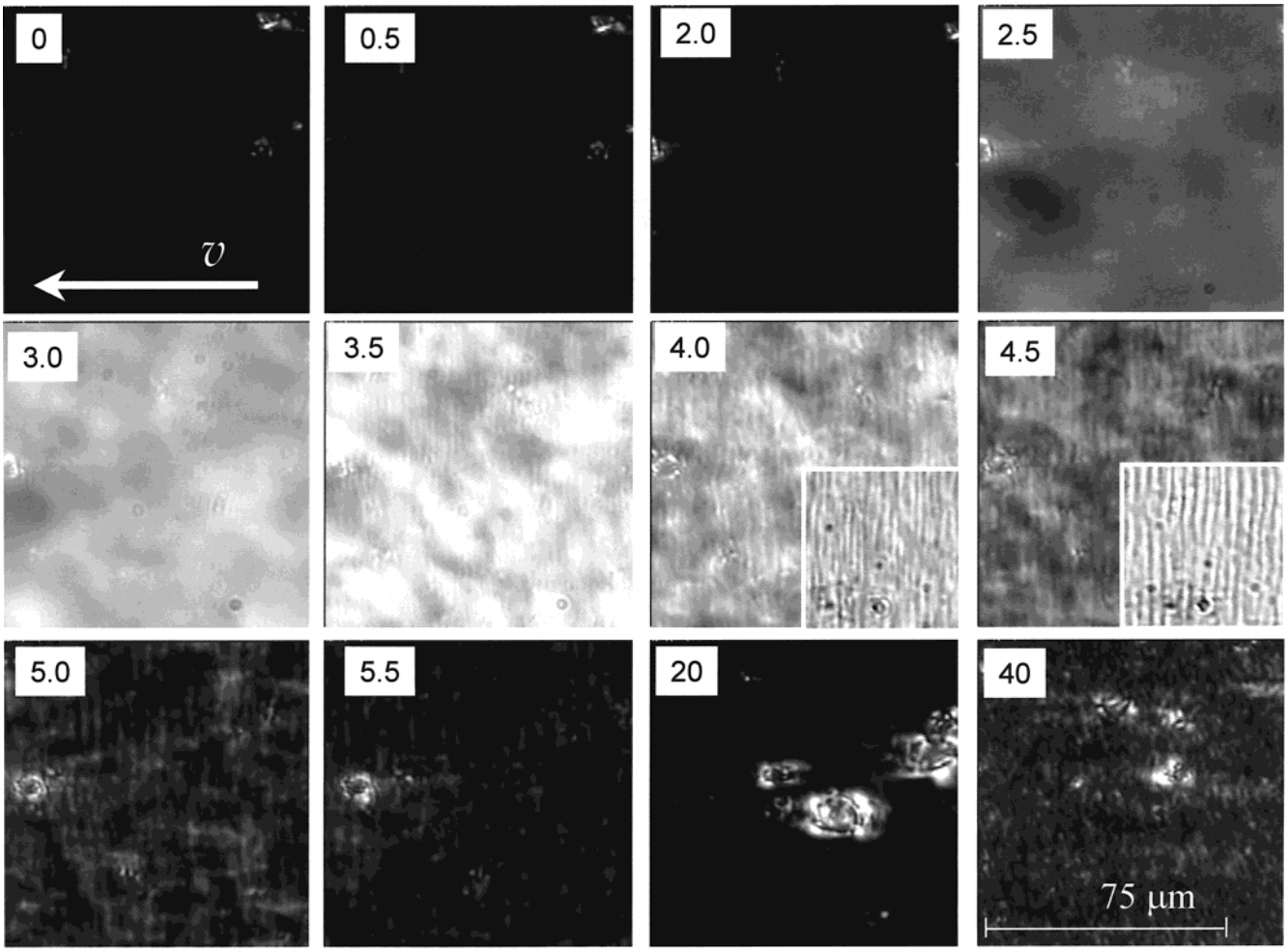

Figure 7. Time evolution of POM image of PSHQ10 at 160 °C and $\dot{\gamma} = 0.5\ s^{-1}$ during a period of 40 s following flow reversal, showing significant light transmission and formation of optical bands. The observation times in seconds are shown in the upper left of each POM image. The optical conditions are the same as those given in Figure 4. The lower right inset micrographs for $t = 4.0$ and 4.5 s used crossed polarizers with the polarizer making an angle of $\pi/4$ with the flow direction.

hesitation, or local maximum, following reversal is quite reproducible under the conditions specified and appears to be a salient feature of these materials. The birefringence data, $\Delta n^+(\dot{\gamma}, t)$, shows a remarkable series of oscillations, indicating a strong reversal-induced disruption of nematic alignment. These oscillations of $\Delta n^+(\dot{\gamma}, t)$ with an amplitude of about 0.02 are superposed on a large undershoot of magnitude 0.06. The oscillations and the undershoot last for a period of nearly 3 min (90 strain units). In contrast, the amplitude of $A_S{}^+(\dot{\gamma}, t)$ shows no high-frequency oscillations, but instead only a broad undershoot (∼0.25), strongly correlated with the large birefringence undershoot. We wish to emphasize the prominent feature of the material's oscillatory response to reversal; namely, the appearance of 2−3 minima in birefringence occurring over the course of 50−100 strain units. However, the magnitude (depth) and precise positioning (strain units following reversal) of the birefringence peaks and valleys vary somewhat from one experiment to the next, even under ostensibly identical conditions.

Shown in Figure 7 are POM images taken for increasing times following flow reversal. Immediately following reversal, the transmitted intensity is negligible and remains so until ≈2.5 s (1.25 strain units) have elapsed, at which point the POM image appears light gray and featureless. Over the course of the next 5−7 s, the POM pattern traverses a bright maximum in transmitted intensity while two textural patterns appear and decay, superimposed on one another. The first texture is relatively coarse with a characteristic length scale refining from 40 μm ($t = 3$ s) to 10 μm ($t = 5$ s) and features no preferred orientation. The second texture consists of bright/dark alternating bands well oriented in the direction perpendicular to the flow axis. These bands feature a characteristic spacing on the order of 10 μm, which is significantly smaller than the sample thickness of 50 μm. The contrast of the second, banded, texture is greatly enhanced by rotating the crossed polarizers by an angle of $\pi/4$. This is shown in the lower right-hand micrographs of Figure 8 for $t = 4.0$ and 4.5 s following flow reversal under identical conditions. That the contrast of the larger scale, unoriented, texture is higher for the case of H_V polarization indicates that orientation of the nematic within these "domains" oscillates spatially about a direction closely parallel to the flow axis. With reference to Figure 3, the band formation occurs and subsides within only the early portion of the birefringence oscillations and the disappearance of the bands coincides closely with the hesitation in shear stress occurring at 5 strain units after reversal. The continued oscillations in birefringence are not related to band formation, but are instead characterized by oscillations between textural states similar to $t = 20$ s (homogeneous, high Δn) and $t = 40$ s (mottled, low Δn) of Figure 7, a finding determined by

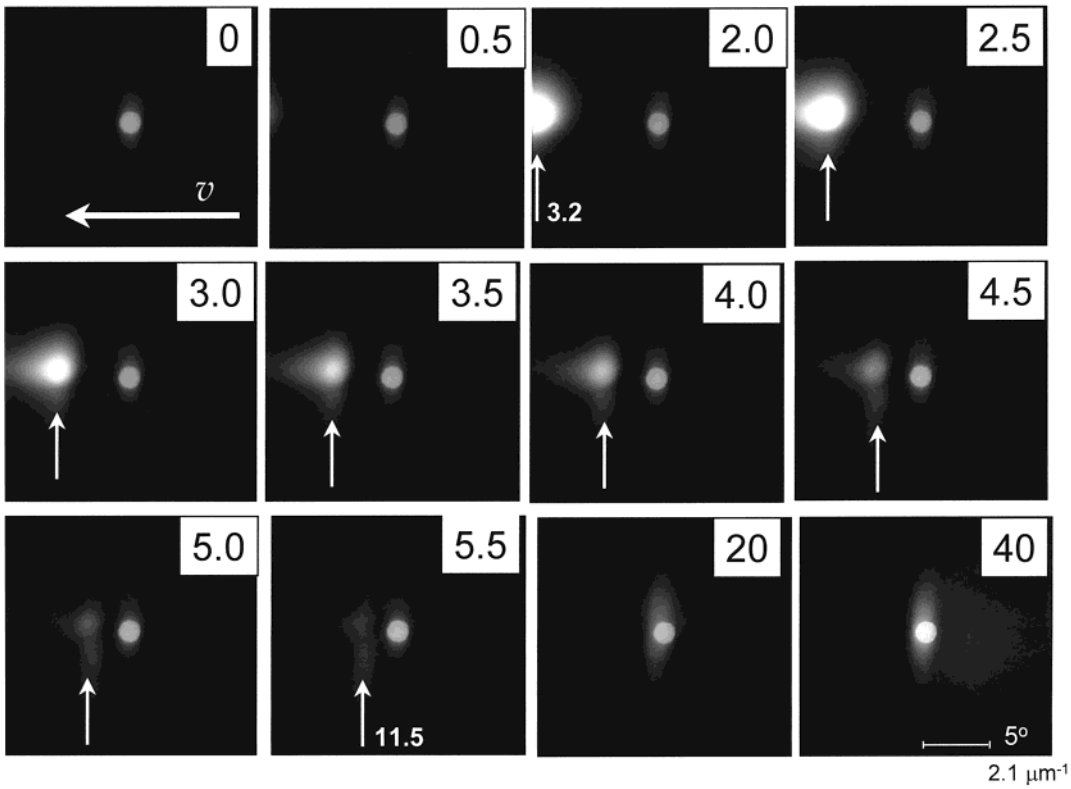

Figure 8. Time evolution of CSALS patterns of PSHQ10 upon flow reversal at 160 °C and $\dot{\gamma} = 0.5\ s^{-1}$. The polarizer is oriented in the flow direction and the analyzer is crossed with the polarizer. The velocity is from right to left with the top plate moving and the receiving optics positioned above the moving plate. Scattering angular range of 5° is indicated with a white bar and the observation times in seconds are shown in the upper right of each POM image. Sample thickness is 50.8 μm.

direct POM observations not shown here. Finally, at long times, the POM images indicate strong orientation along the flow direction.

Figure 8 gives a time series of H_V CSALS patterns of PSHQ10 upon flow reversal, revealing surprising *asymmetric diffraction* in which a single diffraction spot first appears at an angle of ≈10° (on the flow direction side of the incident beam axis) and subsequently translates toward a zero scattering angle as flow in the reverse direction achieves a strain of only 2−3 strain units. For the entire evolution of the diffraction pattern, from inception to disappearance, we have not observed higher order peaks, nor do any peaks to the right of the optical axis appear. Also, the intensity of the diffraction peak decreases monotonically as time passes. All of these characteristics of the CSALS patterns point to the possibility that the reversal of shearing direction results in transient bands, as shown in Figure 7, which act collectively as the optical equivalent of a slanted (or inclined) Bragg diffraction grating following eq 5. The propagation in reciprocal space of the diffraction peak toward zero angle (as highlighted by the arrows in Figure 8 and d values in μm units) indicates a coarsening of the band size and spacing, consistent with direct visualization in Figure 7, while the grating apparently remains slanted as indicated by the continued lack of a second peak on the opposite side of the optical axis.

To further test the hypothesis that the transient bands formed during the flow reversal of PSHQ10 are acting as a Bragg transmission diffraction grating, we have measured the angular position of the diffraction peak as a function of time for two wavelengths of light: 530 nm (open circles) and 480 nm (filled circles) measured during separate experiments. We then calculated

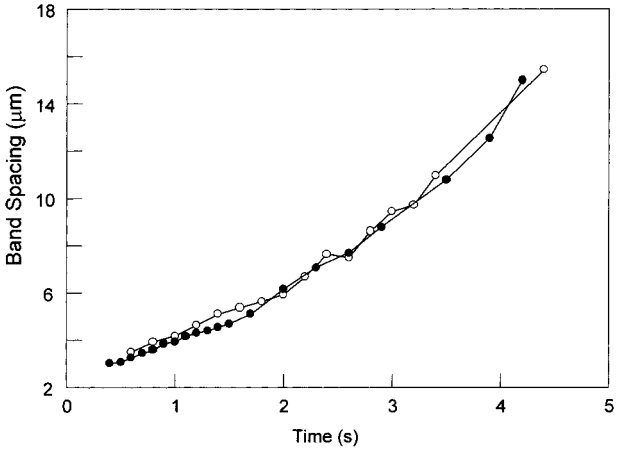

Figure 9. Plot of band spacing versus time upon flow reversal of PSHQ10 using illumination with $\lambda = 480$ nm (●) and $\lambda = 530$ nm (○). The data are taken from CSALS observations under the same shear conditions as those in Figure 8.

the evolution of band spacing (d) from the change in scattering angle using the Bragg formula in transmission (eq 5) with the order, m, set to unity. The results are plotted in Figure 9, where we see an excellent agreement between the two probing wavelengths. This suggests that the Bragg relation holds to describe the evolution of band spacing during flow reversal of a TLCP. Moreover, inspection of Figure 9 reveals favorable consistency with the band sizes observed directly in Figure 7 as well as the suggestion of a finite bands spacing at the time of their creation. This spacing appears to be between 2 and 4 μm.

For comparison to the behavior of PSHQ10, we have examined the rheo-optical response to shear start-up

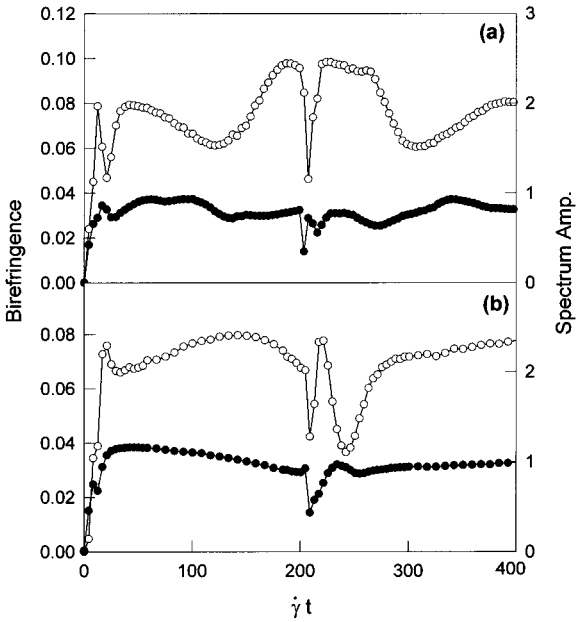

Figure 10. (a) Time evolution of birefringence (○) and spectrum amplitude (●) during shear start-up and flow reversal of PSHQ6 at 210 °C and at $\dot{\gamma} = 0.5$ s^{-1}. Sample thickness is 50.8 μm. (b) Time evolution of birefringence (○) and spectrum amplitude (●) during shear start-up and flow reversal of PSHQ6 at 210 °C and $\dot{\gamma} = 0.1$ s^{-1}. Sample thickness is 50.8 μm.

and reversal of both PSHQ6 and PSHQ11. Figure 10a gives plots of birefringence ($\Delta n^+(\dot{\gamma}, t)$) and spectrum amplitude ($A_S{}^+(\dot{\gamma}, t)$) of PSHQ6 versus time during start-up of shear flow and subsequent flow reversal at 210 °C and at $\dot{\gamma} = 0.5$ s^{-1}. We note that similar to PSHQ10, the peak value of $\sigma^+(\dot{\gamma}, t)$ (not shown) is about 4 times the steady-state shear stress value prior to flow reversal, but that the steady-state shear viscosity is significantly less at 1600 Pa s (compared to ~4800 Pa s for PSHQ10). This difference in steady-state shear viscosity between PSHQ10 and PSHQ6 is attributed to both a significant difference in temperature above glass transition at a fixed temperature below T_{NI} (100 °C for PSHQ6 versus 68 °C for PSHQ10) and to a difference in molecular weight (see Table 1 for the intrinsic viscosities of PSHQ6 and PSHQ10). More importantly, PSHQ6 exhibits a qualitatively distinct response to shear start-up, compared to PSHQ10 observed in Figure 3, with respect to the evolution of birefringence, $\Delta n^+(t)$. In particular, we find, reproducibly, dramatic oscillations in birefringence precluding achievement of a steady level of birefringence, at least up to an accumulated strain of 200 strain units. Despite this observation, the evolution of the spectrum amplitude, $A_S{}^+(\dot{\gamma}, t)$, follows a form similar to that observed for PSHQ10 in Figure 3, though with a slightly accelerated rise to high A_S values. Additionally, there is a lack of correlation between $\Delta n^+(\dot{\gamma}, t)$ and $\sigma^+(\dot{\gamma}, t)$.

In response to a reversal in flow direction for PSHQ6, the shear stress quickly changes sign and achieves steady state, while the birefringence drops dramatically in a transient fashion, followed by strong oscillations similar to the oscillation observed during shear start-up. Indeed, the oscillations appear to simply reverse the start-up response, though not completely. We note that, previously, Mather et al.[43] reported a reversal of oscillatory optical response following a reversal in flow direction for a *tumbling* small-molecule nematic, 8CB, in torsional shearing flow. As we will now show with an example, the reversal in oscillatory optical response (in PSHQ6) only occurs for shear rates above which no steady state can be achieved.

Previously, Kim and Han[20] have shown that shear start-up of PSHQ10 at temperatures significantly below the T_{NI} of that polymer resulted in strong (albeit coherent) oscillations of the first normal stress, which persisted for strains in excess of 500 strain units. Moreover, the duration of the normal stress oscillations was seen to increase with increasing shear rate and decrease with increasing temperature toward T_{NI}. Given these previous observations on PSHQ10, we examined $\Delta n^+(\dot{\gamma}, t)$ for PSHQ6 at the same temperature ($T = 210$ °C), but for a lower shear rate of 0.1 s^{-1}, anticipating enhanced stability of the molecular orientation as probed with $\Delta n^+(\dot{\gamma}, t)$. The results are shown in Figure 10b, where we observe responses to shear start-up and reversal more closely resembling the response of PSHQ10 at $\dot{\gamma} = 0.5$ s^{-1}. Thus it is apparent that, for PSHQ6, decreasing the shear rate increases the stability of birefringence (i.e., alignment) in shear flow. The achievement of a steady-state alignment as observed with birefringence under these conditions is consistent with previous findings of Chang and Han[25] in which PSHQ6 sheared at 0.1 s^{-1} and at $T = 210$ °C reached steady shear and first normal stress values after shearing for ≈100 strain units. The possibility of a rheological transition in this TLCP with increasing shear rate is intriguing and deserves further detailed investigation using optical and mechanical probes.

Reversing the direction of flow for PSHQ6, whether using $\dot{\gamma} = 0.5$ s^{-1} or $\dot{\gamma} = 0.1$ s^{-1}, led to the formation of transient bands quite similar to those seen for PSHQ10 in Figure 7. For example, Figure 11 shows a sequence of H_V POM images for PSHQ6 of 25.4-μm thickness and sheared at 0.5 s^{-1} taken by exposing high-speed color film at times specified on each image in seconds following reversal. It can be seen clearly that bands form quickly following reversal and that the banded pattern is disrupted through interesting domain stretching (12 s) and subsequent domain-size refinement (20 s). We feel that these pictures favorably compare with the predicted tubular inversion wall due to Han and Rey,[13] but a rigorous comparison is beyond the scope of our present study.

Figure 12a,b shows the rheo-optical responses of PSHQ11 at $T = 127$ °C to shearing at 0.5 and 0.1 s^{-1}, respectively, revealing noteworthy findings. First, we observe that the shear stress generated during flow is comparable (for $\dot{\gamma} = 0.5$ s^{-1}) to that of PSHQ10 and larger than PSHQ6 (not presented here). Second, we can see clearly that PSHQ11 features both high magnitude ($\Delta n \sim 0.16$) and stability of birefringence for both high and low shear rates, consistent with previous observations of PSHQ11 mechanical rheology[25] at 0.1 s^{-1} and new results presented below. For both shear rates, PSHQ11 was seen to exhibit transient band formation following flow reversal, much like that seen for PSHQ10 in Figure 7 and PSHQ6 in Figure 11.

3.3. Rheological Response to Shear Start-up. In the present study, using a cone-and-plate rheometer (Rheometrics Scientific Inc., Model RMS 800), we conducted transient shear flow experiments to observe whether transient shear stress $\sigma^+(t, \dot{\gamma})$ and transient first normal stress difference $N_1{}^+(t, \dot{\gamma})$, respectively, scale with shear strain $\dot{\gamma}t$. Accordingly, Figure 13 gives

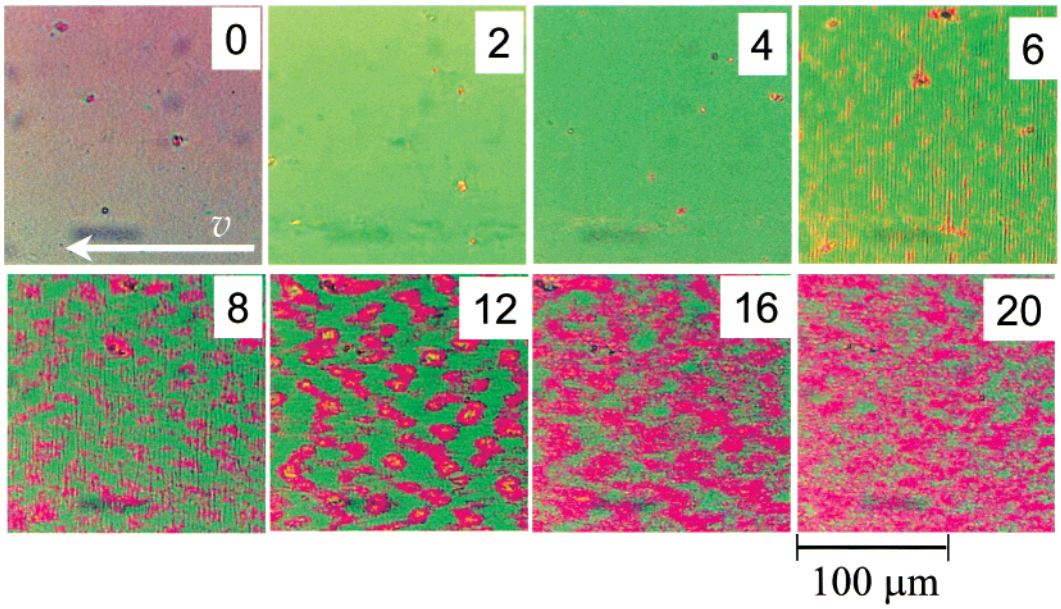

Figure 11. Time evolution of POM images for PSHQ6 upon flow reversal at 160 °C and $\dot{\gamma} = 0.5$ s^{-1}. The flow direction is from right to left and the crossed polarizers are oriented 45° to the flow direction. The observation times in seconds are shown in the upper right of each POM image. Sample thickness is smaller, 25.4 μm.

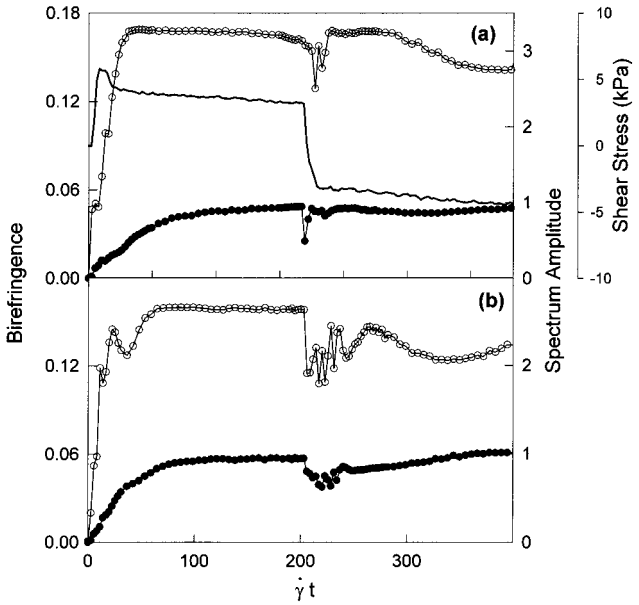

Figure 12. (a) Time evolution of birefringence (○), spectrum amplitude (●), and shear stress (—) during shear start-up and flow reversal of PSHQ11 at 127 °C and at $\dot{\gamma} = 0.5$ s^{-1}. Sample thickness is 50.8 μm. (b) Time evolution of birefringence (○) and spectrum amplitude (●) during shear start-up and flow reversal of PSHQ11 at 127 °C and at $\dot{\gamma} = 0.1$ s^{-1}. Sample thickness is 50.8 μm.

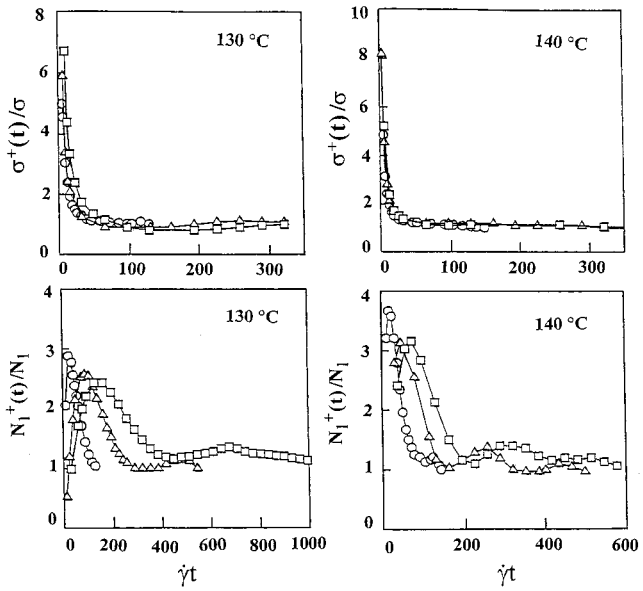

Figure 13. Plots of $\sigma^+(\dot{\gamma}, t)/\sigma$ versus $\dot{\gamma}t$ and $N_1^+(\dot{\gamma}, t)/N_1$ versus $\dot{\gamma}t$ upon shear start-up at 130 and 140 °C for PSHQ10 at three different shear rates: (○) $\dot{\gamma} = 0.107$ s^{-1}; (△) $\dot{\gamma} = 0.536$ s^{-1}; (□) $\dot{\gamma} = 1.07$ s^{-1}.

plots of the ratio $\sigma^+(t, \dot{\gamma})/\sigma$ versus $\dot{\gamma}t$ and the ratio $N_1^+(t, \dot{\gamma})/N_1$ versus $\dot{\gamma}t$ for PSHQ10 at 130 and 140 °C, respectively, for three different shear rates: 0.107, 0.536, and 1.07 s^{-1}. Here, σ denotes the shear stress at steady state and N_1 denotes the first normal stress difference at steady state. Similar plots were obtained, though not presented here, for PSHQ11 and PSHQ6. It should be pointed out that the transient shear flow experiments performed at 130 and 140 °C are in the nematic region ($T_{NI} = 181$ °C for PSHQ10). It can be seen in Figure 13 that the shear stress exhibits a very large overshoot, at strain values close to zero, and then decays very quickly to a steady state. In contrast, the first normal stress difference exhibits a very large overshoot followed by decay with significant oscillations. Particularly noteworthy in Figure 13 is our finding that the ratio $\sigma^+(t, \dot{\gamma})/\sigma$ scales with $\dot{\gamma}t$, while the ratio $N_1^+(t, \dot{\gamma})/N_1$ does *not*. We are not aware of any previous study that investigated whether shear stress and first normal stress difference scale with strain for TLCPs during transient shear flow.

However, in the past some research groups investigated whether shear stress and first normal stress difference scale with strain for lyotropic solutions during transient shear flow. Moldenaers et al.[14] employed a lyotropic solution of 12 wt % poly(benzyl-L-glutamate) (PBLG) in *m*-cresol, Picken et al.[41] employed a lyotropic solution of 19.8 wt % poly(*p*-phenyleneterephthalamide) in sulfuric acid, and Mewis and Moldenaers[44] also

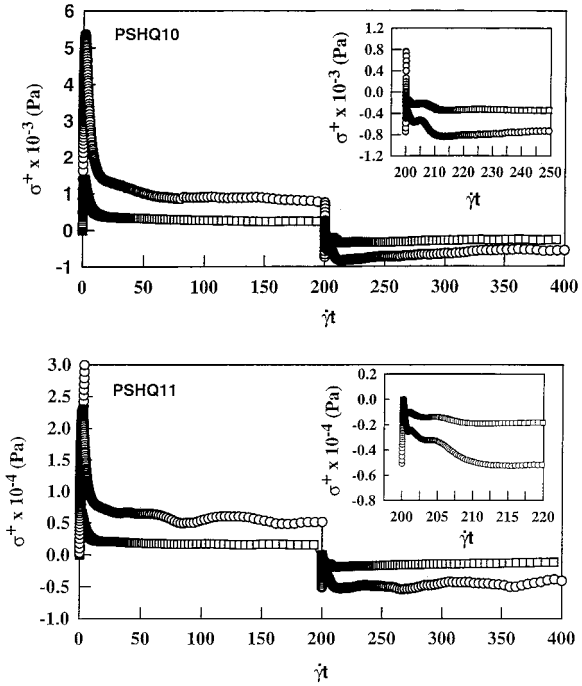

Figure 14. Plots of $\sigma^+(\dot{\gamma}, t)$ versus $\dot{\gamma}t$ upon shear start-up followed by flow reversal for PSHQ10 at 160 °C for (□) $\dot{\gamma}$ = 0.1 s^{-1} and (○) $\dot{\gamma}$ = 0.5 s^{-1} and PSHQ11 at 127 °C for (□) $\dot{\gamma}$ = 0.1 s^{-1} and (○) $\dot{\gamma}$ = 0.5 s^{-1}. Flow reversal began after 200 strain units upon shear start-up. Note that T_{NI} = 181 °C for PSHQ10 and T_{NI} = 147 °C for PSHQ11.

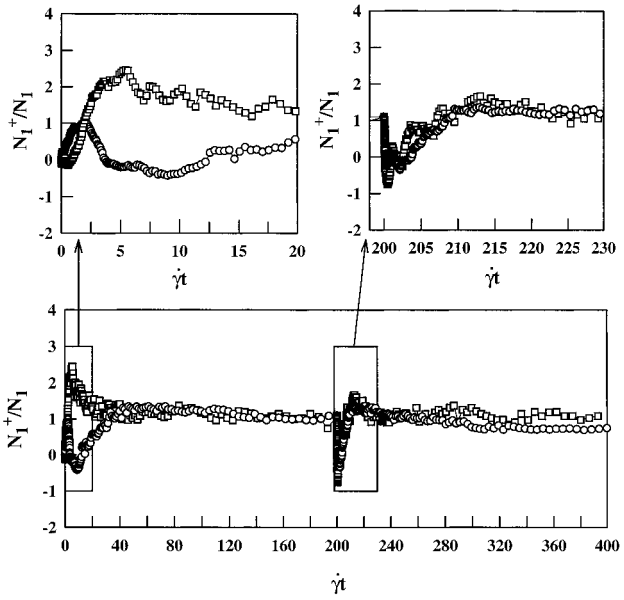

Figure 15. Plots of $N_1^+(\dot{\gamma}, t)/N_1$, where N_1 is the steady-state value, versus $\dot{\gamma}t$ at 160 °C, upon shear start-up followed by flow reversal, for PSHQ10 at two different shear rates: (□) $\dot{\gamma}$ = 0.1 s^{-1} and (○) $\dot{\gamma}$ = 0.5 s^{-1}. Flow reversal began after 200 strain units upon shear start-up. Note that T_{NI} = 181 °C for PSHQ10.

employed a lyotropic solution of 12 wt % PBLG in *m*-cresol. These investigators[14,41,44] observed that the ratio $\sigma^+(t, \dot{\gamma})/\sigma$ scaled with $\dot{\gamma}t$ during transient shear flow. On the other hand, Grizzuti et al.[45] who employed lyotropic solutions of hydroxypropyl cellulose (HPC) in water, and Walker et al.[46] who employed a lyotropic solution of 40 wt % PBLG in *m*-cresol, observed *failure* of strain scaling for the ratio $\sigma^+(t, \dot{\gamma})/\sigma$ during transient shear flow. It is then fair to state that there is *no* general expectation for strain scaling of shear stress, even for lyotropic LCPs during transient shear flow.

Concerning the scaling of first normal stress difference with strain, very few research groups have investigated this problem for lyotropic solutions during transient shear flow and apparently no work has addressed the issue for TLCPs. Walker et al.[46] observed success of strain scaling for the ratio $N_1^+(t, \dot{\gamma})/N_1$ for a lyotropic solution of 40 wt % PBLG in *m*-cresol during transient shear flow. Thus, comparison with our experimental results (Figure 13), where failure of strain scaling for $N_1^+(t, \dot{\gamma})/N_1$ is observed for a semiflexible main-chain TLCP (PSHQ10), reveals (not surprisingly) distinct behavior between the two material systems. Thus, we can conclude that there is *no* general expectation for strain scaling of first normal stress difference data for LCPs during transient shear flow.

3.4. Rheological Responses to Flow Reversal. In the present study, using a cone-and-plate rheometer (Rheometrics Scientific Inc., Model ARES) we conducted flow reversal experiments by suddenly changing the direction of shear flow after 200 strain units upon shear start-up. Figure 14 reveals the responses of shear stress $\sigma^+(t, \dot{\gamma})$ to shear start-up for the first 200 strain units and to flow reversal for the next 200 strain units for PSHQ10 at 160 °C (a higher temperature than that used in Figure 13, but the same as that of Figure 3) and for PSHQ11 at 127 °C (see Figure 12), respectively, at two different shear rates: 0.1 and 0.5 s^{-1}. It can be seen in Figure 14 that, upon shear start-up, $\sigma^+(t, \dot{\gamma})$ increases very rapidly, exhibiting a very large overshoot, and then decays very quickly to a steady state. It is of interest to observe in Figure 14 that $\sigma^+(t, \dot{\gamma})$ for PSHQ11 at $\dot{\gamma}$ = 0.5 s^{-1} shows a mild oscillatory decay during the entire 200 strain units, while no such oscillatory decay is observed at $\dot{\gamma}$ = 0.1 s^{-1}. Upon flow reversal, in Figure 14 we observe a minor overshoot in $\sigma^+(t, \dot{\gamma})$ (see the inset) for both PSHQ10 and PSHQ11 for the two different shear rates. These observations are in agreement with those made from the optical microrheometer for PSHQ10 at 160 °C and $\dot{\gamma}$ = 0.5 s^{-1} (Figure 3a). It can easily be surmised from Figure 14 that the ratio $\sigma^+(t, \dot{\gamma})/\sigma$ scales with $\dot{\gamma}t$, after the reversal in flow direction.

In the lower panel of Figure 15 are given the responses of $N_1^+(t, \dot{\gamma})$, normalized by the steady-state value (N_1), to shear start-up for the first 200 strain units and to flow reversal for the next 200 strain units for PSHQ10 at 160 °C for two different shear rates, 0.1 and 0.5 s^{-1}. To help observe the details of the overshoot and undershoot in the early stage of shear start-up and flow reversal, in the upper panel of Figure 15 are given the responses of $N_1^+(t, \dot{\gamma})/N_1$ for the first 20 strain units upon shear start-up and for the first 30 strain units upon flow reversal. The following observations are worth noting in Figure 15. Upon shear start-up, $N_1^+(t, \dot{\gamma})/N_1$ for $\dot{\gamma}$ = 0.5 s^{-1} initially increases very rapidly, exhibiting a very large overshoot, is followed by a very large undershoot featuring negative N_1 values, and then increases again followed by a series of oscillations, whereas the $N_1^+(t, \dot{\gamma})/N_1$ at $\dot{\gamma}$ = 0.1 s^{-1} goes through a maximum and decays with oscillations. Upon flow reversal, the $N_1^+(t, \dot{\gamma})/N_1$ for both shear rates, 0.1 and 0.5 s^{-1}, exhibits both an overshoot and undershoot, with the magnitude of the overshoot at 0.5 s^{-1} being even greater than that upon shear start-up.

It is interesting to compare the normal stress transients for PSHQ11 with those of PSHQ10. In the lower

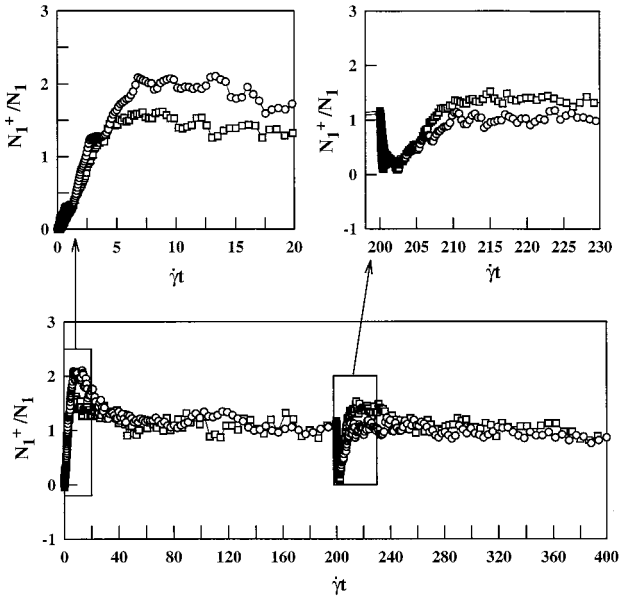

Figure 16. Plots of $N_1^+(\dot{\gamma}, t)/N_1$, where N_1 is the steady-state value, versus $\dot{\gamma}t$ at 127 °C, upon shear start-up followed by flow reversal, for PSHQ11 at two different shear rates: (□) $\dot{\gamma} = 0.1$ s^{-1} and (○) $\dot{\gamma} = 0.5$ s^{-1}. Flow reversal began after 200 strain units upon shear start-up. Note that $T_{NI} = 147$ °C for PSHQ11.

panel of Figure 16 are given the responses of $N_1^+(t, \dot{\gamma})/N_1$ to shear start-up for the first 200 strain units and to flow reversal for the next 200 strain units for PSHQ11 at 127 °C and at two different shear rates, 0.1 and 0.5 s^{-1}. To help observe the details of the responses of $N_1^+(t, \dot{\gamma})/N_1$ in the early stage of shear start-up and flow reversal, in the upper panel of Figure 16 are given the responses of $N_1^+(t, \dot{\gamma})/N_1$ for the first 20 strain units upon shear start-up and for the first 30 strain units upon flow reversal. In contrast to the observations made in Figure 15 for PSHQ10, shear start-up and reversal for PSHQ11 result in only a mild overshoot of $N_1^+(t, \dot{\gamma})/N_1$, which decays very slowly with oscillations at both shear rates, 0.1 and 0.5 s^{-1}. That is, *no* negative transient $N_1^+(t, \dot{\gamma})$ is observed in PSHQ11, in contrast to PSHQ10.

We would like to highlight the qualitative similarity in transient behavior, upon flow reversal, between the $N_1^+(t, \dot{\gamma})$ observed using a cone-and-plate rheometer (Figures 15 and 16) and the birefringence $\Delta n^+(t, \dot{\gamma})$ observed using our optical microrheometer (Figure 3a,b for PSHQ10 and in Figure 12 for PSHQ11). It is interesting to observe in Figures 15 and 16 that the first normal stress difference clearly does not scale with $\dot{\gamma}t$ for the TLCPs during transient shear flow but shows reasonable scaling with strain (when normalized by the steady value) for data following the reversal in flow direction. We are not aware of any previous study that investigated whether first normal stress difference scales with strain for TLCPs after a reversal in flow direction.

In the past, however, a few research groups investigated strain scaling of shear stress for lyotropic solutions after the reversal in flow direction. Moldenaers et al.[14] observed that the ratio $\sigma^+(t, \dot{\gamma})/\sigma$ scaled with $\dot{\gamma}t$ after the reversal in flow direction has occurred in a lyotropic solution of 12 wt % PBLG in *m*-cresol. A similar observation was made by Burghardt and Fuller[47] who employed lyotropic solutions of PBG in *m*-cresol. On the other hand, Hongladarom et al.[15] did *not* observe strain scaling with the ratio $\sigma^+(t, \dot{\gamma})/\sigma$ for lyotropic solutions of HPC in water after the reversal in flow direction. Walker et al.[46] have observed strain scaling with the ratio $\sigma^+(t, \dot{\gamma})/\sigma$ for a lyotropic solution of 37 wt % PBLG in *m*-cresol and in a separate work for concentrations spanning 12−37% in *m*-cresol,[48] but *not* for a lyotropic solution of 40 wt % PBLG in *m*-cresol, after the reversal in flow direction. However, the latter result can now be attributed to the formation of a hexagonally packed ordered phase at such high concentrations.[49] It is then fair to state that no general conclusion can be drawn concerning strain scaling of shear stress for LCPs after the reversal in flow direction.

There are, additionally, very few papers dealing with strain scaling of first normal stress difference data for lyotropic LCPs after reversal in flow direction. Chow et al.[17] reported variations of $N_1^+(\dot{\gamma}, t)$ with $\dot{\gamma}t$ for lyotropic solutions of poly(*p*-phenylenebenzobisthiazole) (PBZT) after the reversal in flow direction, indicating that, for this system, first normal stress difference does not follow strain scaling after flow reversal. Subsequently, Walker et al.[48] reported that strain scaling of N_1 data for PBLG solutions in *m*-cresol does apply when shear rates in "region II" were used. The reversal N_1 data followed a marked undershoot followed by damped oscillations to steady values. In light of these limited data, our experimental results (Figures 15 and 16) for semiflexible main-chain TLCPs (PSHQ10 and PSHQ11) tend to agree more closely with those of Walker on PGLB solutions than with those of Chow et al.[17] on PBZT solutions.

In the present study, we investigated whether the ratio $N_1^+(t, \dot{\gamma})/\sigma^+(t, \dot{\gamma})$ obtained from a cone-and-plate rheometer might scale with $\dot{\gamma}t$ for PSHQ10 and PSHQ11, based on our previous observations indicating correlation between the ratio $N_1^+(t, \dot{\gamma})/\sigma^+(t, \dot{\gamma})$ and $\Delta n^+(t, \dot{\gamma})$ during transient shear flow of segmented main-chain TLCPs with varying pendant side groups.[50] For this, we employed the data displayed in Figures 14−16 to prepare plots of $N_1^+(t, \dot{\gamma})/\sigma^+(t, \dot{\gamma})$ versus $\dot{\gamma}t$, and they are given in Figure 17 for PSHQ10 and in Figure 18 for PSHQ11 after the reversal in the flow direction. In the upper panel of Figure 17 are given the variations of $N_1^+(t, \dot{\gamma})/\sigma^+(t, \dot{\gamma})$ with $\dot{\gamma}t$ for the first 20 strain units upon flow reversal of PSHQ10, and in the upper panel of Figure 18 are given the variations of $N_1^+(t, \dot{\gamma})/\sigma^+(t, \dot{\gamma})$ with $\dot{\gamma}t$ for the first 20 strain units upon flow reversal of PSHQ11. Upon comparing Figure 17 with Figure 3 for PSHQ10 and Figure 18 with Figure 12 for PSHQ11, it is observed that a qualitative similarity exists between the oscillatory behavior of the ratio $N_1^+(t, \dot{\gamma})/\sigma^+(t, \dot{\gamma})$ and the oscillatory behavior of $\Delta n^+(t, \dot{\gamma})$, consistent with our observation made for segmented main-chain TLCPs with varying pendant side groups.[50] From Figures 17 and 18 we observe that the ratio $N_1^+(t, \dot{\gamma})/\sigma^+(t, \dot{\gamma})$ does not scale rigorously with $\dot{\gamma}t$, although a general trend exists, for both PSHQ10 and PSHQ11 after the reversal in flow direction.

Earlier, Hongladarom and Burghardt[51] reported that $\Delta n^+(t, \dot{\gamma})$ scaled with $\dot{\gamma}t$ during reversal flow of lyotropic solutions of PBG. Specifically, they observed an oscillatory behavior of $\Delta n^+(t, \dot{\gamma})$, independent of the previously applied $\dot{\gamma}$, in the low shear-rate regime and then concluded that the presence of oscillations of $\Delta n^+(t, \dot{\gamma})$ was a consequence of director tumbling. On the other hand, Hongladarom and Burghardt also reported[15] that $\Delta n^+(t, \dot{\gamma})$ did *not* scale with $\dot{\gamma}t$ during reversal flow of

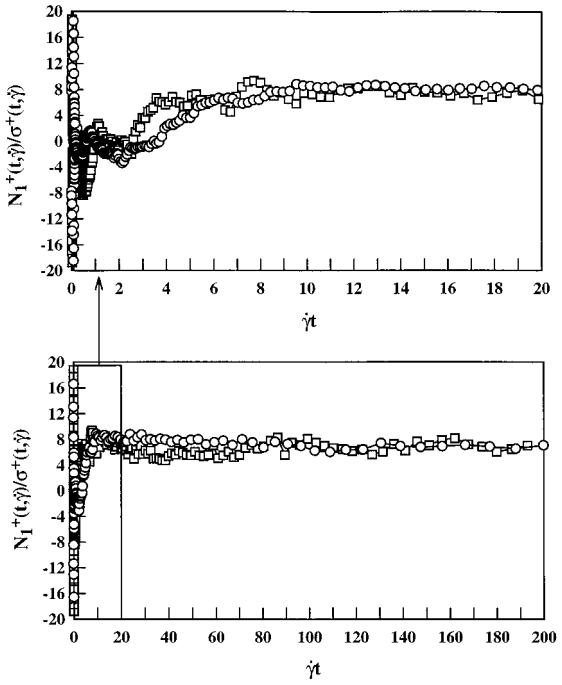

Figure 17. Plots of $N_1^+(\dot\gamma, t)/\sigma^+(\dot\gamma, t)$ versus $\dot\gamma t$ at 160 °C, after the reversal in flow direction, for PSHQ10 at two different shear rates: (□) $\dot\gamma = 0.1\ s^{-1}$ and (○) $\dot\gamma = 0.5\ s^{-1}$.

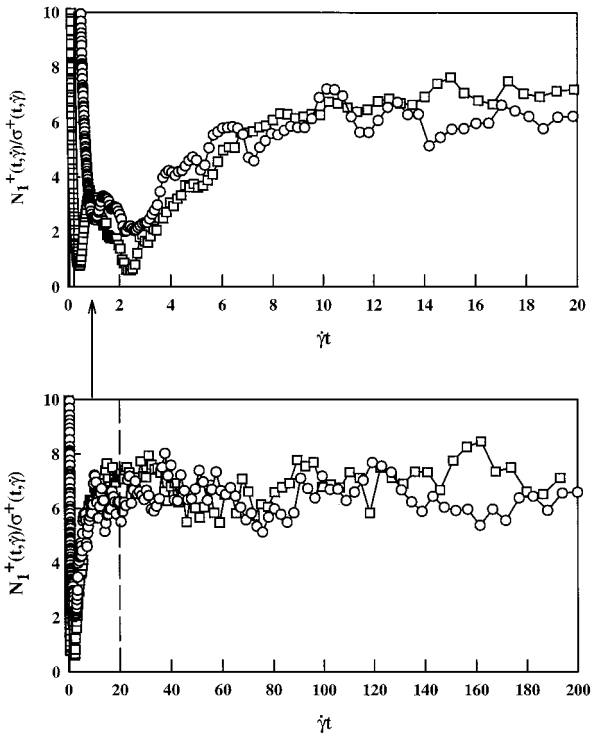

Figure 18. Plots of $N_1^+(\dot\gamma, t)/\sigma^+(\dot\gamma, t)$ versus $\dot\gamma t$ at 127 °C, after the reversal in flow direction, for PSHQ11 at two different shear rates: (□) $\dot\gamma = 0.1\ s^{-1}$ and (○) $\dot\gamma = 0.5\ s^{-1}$.

lyotropic solutions of HPC in water. They speculated that within the low shear-rate regime the domains might interact more strongly with one another, perhaps through distortional elasticity, so that hydrodynamic torques rotating the director become less effective. The lack of quantitative strain scaling for the ratio $N_1^+(t, \dot\gamma)/\sigma^+(t, \dot\gamma)$ after the reversal in flow direction, as observed in Figures 17 and 18, may similarly be attributable to the dominance of distortional elasticity in the rheological response. Again, it is fair to state that no general conclusion can be drawn on strain scaling for first normal stress difference for LCPs after the reversal in flow direction.

4. Concluding Remarks

In this study the micrometer-scale microstructure and molecular-scale ordering during shear start-up followed by reversal flow were measured in-situ using microscopy, light scattering, and birefringence methods. To date, relatively few studies have been reported on simultaneous measurements of morphology and rheology, upon shear start-up followed by flow reversal, of semiflexible main-chain TLCPs. The study reported in this paper may be the first serious effort spent on a better understanding at a fundamental level about interrelationships between the morphology and rheology of semiflexible main-chain TLCPs during both shear start-up and flow reversal. Specifically, from our rheo-optical observations, we have determined that while all the PSHQ*n* materials studied feature band formation upon flow reversal, a qualitative distinction exists between the polymer with a shorter spacer length, PSHQ6, and the polymers with longer spacer lengths, PSHQ10 and PSHQ11.

During the past 2 decades, several research groups[19,52−57] developed constitutive equations to predict the rheological behavior of lyotropic LCPs, but relatively little effort has been spent on predicting the rheological behavior of TLCPs. One of the most important features of semiflexible main-chain TLCPs, which distinguishes them from lyotropic LCPs, lies in the persistent defect-ridden texture that leads to many unusual rheological characteristics, such as (i) strong sensitivity to thermal and deformation histories,[29,30] (ii) a very large initial overshoot and often multiple peaks in first normal stress difference upon shear start-up,[20−23,25] (iii) very slow oscillatory decay of first normal stress difference until reaching a steady-state value upon shear start-up,[20−23,25] (iv) very slow relaxation of first normal stress difference upon cessation of steady shear flow,[24] and (v) very slow and long structure recovery, as determined by an increase in complex viscosity or dynamic loss modulus, upon cessation of steady-state shear flow.[23] Additionally, the present study has shown that even well-aligned samples are subject to micrometer-scale pattern formation (bands) following flow reversal. Granted, prediction of such unusual rheological behavior of TLCPs would be a formidable task indeed; however, very few theoretical studies exist in the literature dealing with predictions of such experimental observations made on semiflexible main-chain TLCPs.

It is worth mentioning at this juncture that earlier Maffettone and Marrucci[58] developed a "nematic dumbbell model" to describe the dynamics of semiflexible, low-molecular-weight (i.e., unentangled) LCPs by incorporating flexibility along the chain backbone, similar to the approach employed in molecular modeling of flexible polymers. They reported that the nematic dumbbell model predicts a flow-alignment behavior in an LCP. We wish to point out that while the nematic dumbbell model predicts only a Newtonian viscosity, PSHQ10 employed in this study, for instance, is an entangled polymer (see Figure 6 in ref 21, where log G' versus log G'' plots having a slope of 2 in the terminal region show molecular-weight independence) and exhibit at least two regimes or three regimes in some cases (depending upon

thermal history and deformation history) in shear viscosity.[21] Further, the TLCPs investigated in this study feature a nematic "polydomain" texture, while the nematic dumbbell model does not describe the polydomain nature of LCPs and neglects the effects of interactions between domains. We thus conclude that while the approach taken by Maffettone and Marrucci[58] appears to be in the right direction, more sophisticated molecular models are needed to describe the dynamics of semiflexible, entangled TLCPs with a nematic texture.

Although the paper by Marrucci and Maffettone[59,60] predicts the appearance of multiple overshoots in first normal stress difference during transient shear flow, their theory is based on a monodomain model that predicts a tumbling behavior and is also based on the Maier−Saupe intermolecular potential (excluded volume interactions).[61] It should be mentioned that the Maier−Saupe excluded-volume potential may be valid for small molecule thermotropic liquid crystals, but certainly not for semiflexible main-chain TLCPs. However, information available in the literature and our unpublished results, Figure 10 of the present work not withstanding, suggest that semiflexible main-chain TLCPs exhibit a flow-aligning behavior and not a tumbling behavior. Ugaz and Burghardt[62] compared experimental results for transient shear flow and flow reversal of model semiflexible main-chain TLCPs with the predictions from the Ericksen polydomain model.[63] Further, Ugaz[64] has very recently compared the experimental results for transient shear flow and flow reversal of model semiflexible main-chain TLCPs with the Larson−Doi mesoscopic model[19] that includes distortional elastic effects. The Larson−Doi mesoscopic model[19] was formulated by taking the spatial average of the Leslie−Ericksen equations[65] over a length scale large enough to encompass the texture size a and still smaller than bulk dimensions. In doing so, Larson and Doi considered the evolution of texture on the basis of some experimental observations that the domain size decreases with increasing shear rate and grows upon cessation of flow.

Although both the Ericksen polydomain model[63] and the Larson−Doi mesoscopic model[19] predicted qualitatively the experimental observations for the time evolution of $\sigma^+(\dot{\gamma}, t)$ and $N_1^+(\dot{\gamma}, t)$ for a model TLCP (PSHQ6−12), during transient shear flow, according to Ugaz,[64] the predicted magnitude of $\sigma^+(\dot{\gamma}, t)$ is lower than that of $N_1^+(\dot{\gamma}, t)$, which is opposite to experimental observations. Additionally, the models predict a somewhat shorter transient time (strain) of shear stress and first normal stress difference variations compared to experimental results. The failure of the Larson−Doi model to accurately predict the time evolution of $N_1^+(\dot{\gamma}, t)$ during transient shear flow of the model TLCP, PSHQ6−12, may be attributed to the presence of long flexible spacers (allowing some entanglement) and the presence of bulky pendant side groups (modifying interchain interactions and intrachain conformation), among many factors. Specifically, both long flexible spacers and bulky pendant side groups present in PSHQ6−12 employed by Ugaz[64] might directly suppress *molecular* rotations and thus, perhaps, collective molecular rotations, or director tumbling.

Because the chemical structures of PSHQ6, PSHQ10, and PSHQ11 employed in this study are very similar to the chemical structure of PSHQ6−12 employed by Ugaz,[64] except that PSHQ6−12 is a copolyester, we expect that predictions of transient shear flow behavior of PSHQ6, PSHQ10, or PSHQ11 by the Larson−Doi model[19] would roughly be the same as those observed by Ugaz.[64] Although the Larson−Doi model[19] is virtually the only model available in the literature that incorporates polydomain texture and distortional elastic effects, the model is based on the Leslie−Ericksen equations, which may be more appropriate for small molecule or lyotropic systems that feature short relaxation times (i.e., fixed local order parameter, S, for typical shear rates). Because the TLCPs investigated in the present study apparently exhibit flow-aligning behavior, which seems to be a distinguishing feature of semiflexible TLCPs, one needs to develop a theory that can accommodate such a feature.

Acknowledgment. P.T.M. acknowledges financial support from the Materials and Manufacturing Directorate of the Air Force Research Laboratory. C.D.H. acknowledges financial support from the National Science Foundation under Grant CTS-9614929.

References and Notes

(1) Dobb, M. G.; Johnson, D. J.; Saville, B. P. *J. Polym. Sci.: Polym. Phys. Ed.* **1977**, *15*, 2201.
(2) Simmens, S. C.; Hearle, J. W. S. *J. Polym. Sci.: Polym. Phys. Ed.* **1980**, *18*, 871.
(3) Viney, C.; Donald, A. M.; Windle, A. H. *J. Mater. Sci.* **1983**, *18*, 1136.
(4) Marrucci, G.; Grizzuti, N.; Buonaurio, A. *Mol. Cryst. Liq. Cryst.* **1987**, *153*, 263.
(5) Maffettone, P. L.; Grizzuti, N.; Marrucci, G. *Liq. Cryst.* **1989**, *4*, 385.
(6) Bedford, S. E.; Windle, A. H. *Polymer* **1990**, *31*, 616.
(7) Hou, J.; Wu, W.; Xu, M.; Li, X. *Polymer* **1996**, *37*, 5205.
(8) Kundler, I.; Finkelmann, H. *Macromol. Chem. Phys.* **1998**, *199*, 677.
(9) Pieranski, P.; Guyon, E. *J. Phys. (Paris)* **1976**, *37*, 3.
(10) Manneville, P.; Dubois-Violette, E. *J. Phys. (Paris)* **1976**, *37*, 285.
(11) Larson, R. G. *J. Rheol.* **1993**, *37*, 175.
(12) Verwey, G. C.; Warner, M.; Terentjev, E. M. *J. Phys. II Fr.* **1996**, *6*, 1273.
(13) Han, W. H.; Rey, A. D. *Macromolecules* **1995**, *28*, 8401.
(14) Moldenaers, P.; Fuller, G.; Mewis, J. *Macromolecules* **1989**, *22*, 960.
(15) Hongladarom, K.; Secakusuma, V.; Burghardt, W. R. *J. Rheol.* **1994**, *38*, 1505.
(16) Burghardt, W. R. *Macromol. Chem. Phys.* **1998**, *199*, 471.
(17) Chow, A.; Hamlin, R. D.; Ylitalo, C. M. *Macromolecules* **1992**, *25*, 7135.
(18) Semenov, A. N. *J. Rheol.* **1993**, *37*, 911.
(19) Larson, R. G.; Doi, M. *J. Rheol.* **1991**, *35*, 539.
(20) Kim, S. S.; Han, C. D. *J. Rheol.* **1993**, *37*, 847.
(21) Kim, C. D.; Han, C. D. *Macromolecules* **1993**, *26*, 6633.
(22) Han, C. D.; Chang, S.; Kim, S. S. *Mol. Cryst. Liq. Cryst.* **1994**, *254*, 335.
(23) Han, C. D.; Kim, S. S. *J. Rheol.* **1994**, *38*, 13.
(24) Han, C. D.; Kim, S. S. *J. Rheol.* **1994**, *38*, 31.
(25) Chang, S.; Han, C. D. *Macromolecules* **1997**, *30*, 2021.
(26) Furukawa, A.; Lenz, R. W. *Macromol. Chem., Macromol. Symp.* **1986**, *2*, 3.
(27) Kim, S. S.; Han, C. D. *Polymer* **1994**, *35*, 93.
(28) Chang, S.; Han, C. D. *Macromolecules* **1997**, *30*, 1670.
(29) Lin, Y. G.; Winter, H. H. *Macromolecules* **1991**, *24*, 2877.
(30) Kim, S. S.; Han, C. D. *Macromolecules* **1993**, *26*, 3176.
(31) Gilmore, J. R.; Colby, R. H.; Hall, E.; Ober, C. K. *J. Rheol.* **1994**, *38*, 1623.
(32) Mather, P. T.; Stüber, H. R.; Chaffee, K. P.; Haddad, T. S.; Romo-Uribe, A.; Lichtenhan, J. D. In *Liquid Crystals for Advanced Technologies*; Chen, S., Bunning, T., Eds.; MRS Symposium Proceedings No. 425; MRS: Washington, DC, 1996; p 137.
(33) Mather, P. T.; Romo-Uribe, A.; Han, C. D.; Kim, S. S. *Macromolecules* **1997**, *30*, 7977.
(34) ImageTool software, formerly available from University of Texas Health Science Center.

(35) Hongladarom, K.; Burghardt, W. R.; Baek, S. G.; Cementwala, S.; Magda, J. J. *Macromolecules* **1993**, *26*, 772.
(36) Beekmans, F.; Posthuma de Boer, A. *Macromolecules* **1996**, *29*, 8726.
(37) Born, M.; Wolf, E. *Principles of Optics*; Pergamon: New York, 1980.
(38) Hsiao, B. S.; Stein, R. S.; Deutcher, K.; Winter, H. H. *J. Polym. Sci. B: Polym. Phys.* **1990**, *28*, 1571.
(39) Romo-Uribe, A.; Mather. P. T.; Chaffee, K. P.; Han, C. D. In *Morphology Control in Polymer Blends*; Briber, R., Han, C. C., Peiffer, D. G, Eds.; MRS Symposium Proceedings No. 461; MRS: New York, 1997; p 64.
(40) Takebe, T.; Hashimoto, T.; Ernst, B.; Navard, P.; Stein, R. S. *J. Chem. Phys.* **1990**, *92*, 1386.
(41) Picken, S. J.; Aerts, J.; Doppert, H. L.; Reuvers, A. J.; Northolt, M. G. *Macromolecules* **1991**, *24*, 1366.
(42) Walker, L. M.; Kernick, W. A., III; Wagner, N. J. *Mcaromolecules* **1997**, *30*, 508.
(43) Mather, P. T.; Pearson, D. S.; Larson, R. G.; Gu, D. F.; Jamieson, A. M. *Rheol. Acta* **1997**, *36*, 485.
(44) Mewis, J.; Moldenaers, P. *Mol. Cryst. Liq. Cryst.* **1987**, *153*, 291.
(45) Grizzuti, N.; Cavella, S.; Cicarelli, P. *J. Rheol.* **1990**, *30*, 1293.
(46) Walker, L. M.; Wagner, N. J.; Larson, R. G.; Mirau, P. A.; Moldenaers, P. *J. Rheol.* **1995**, *39*, 925.
(47) Burghardt, W. R.; Fuller, G. G. *Macromolecules* **1991**, *24*, 2546.
(48) Walker, L. M.; Mortier, M.; Moldenaers, P. *J. Rheol.* **1996**, *40*, 967.
(49) Ugaz, V. M.; Cinader, D. K.; Burghardt, W. R. *J. Rheol.* **1998**, *42*, 379.
(50) Kim, D. O.; Han, C. D.; Mather, P. T. *Macromolecules*, in press.
(51) Hongladarom, K.; Burghardt, W. R. *Macromolecules* **1993**, *26*, 785.
(52) Doi, M. *J. Polym. Sci., Polym. Phys. Ed.* **1981**, *19*, 229.
(53) Doi, M. *Faraday Symp. Chem. Soc.* **1983**, *18*, 49.
(54) Kuzuu, N.; Doi, M. *J. Phys. Soc. (Jpn.)* **1983**, *52*, 3486.
(55) Kuzuu, N.; Doi, M. *J. Phys. Soc. (Jpn.)* **1983**, *53*, 1031.
(56) Larson, R. G.; Mead, D. W. *J. Rheol.* **1989**, *33*, 185.
(57) Larson, R. G.; Mead, D. W. *J. Rheol.* **1989**, *33*, 1251.
(58) Maffettone, P. L.; Marrucci, G. *J. Rheol.* **1992**, *36*, 1547.
(59) Marrucci, G.; Maffettone, P. L. *J. Rheol.* **1990**, *34*, 1217.
(60) Maffettone, P. L.; Marrucci, G. *J. Rheol.* **1990**, *34*, 1231.
(61) Maier, V. W.; Saupe, A. *Z. Naturforsch. Teil A* **1958**, *13A*, 564; **1959**, *14A*, 882; **1960**, *15A*, 287.
(62) Ugaz, V. M.; Burghardt, W. R. *Macromolecules* **1999**, *31*, 8474.
(63) Erickson, J. L. *Arch. Ration. Mech. Anal.* **1960**, *4*, 231.
(64) Ugaz, V. M. Investigation of the Effect of Shear Flow on Molecular Orientation in Model Thermotropic Liquid Crystalline Polymers Using In Situ X-ray Scattering. Doctoral Dissertation, Northwestern University, Evanston, IL, 1999.
(65) Leslie, F. M. In *Advances in Liquid Crystals*; Brown, G. H., Ed.; Academic Press: New York, 1979; Vol. 4, pp 1−80.

MA000765R